frontiers in Energy Research

ORIGINAL RESEARCH
published: 02 September 2020
doi: 10.3389/fenrg.2020.00148

Preparation of Graphene-Like Porous Carbons With Enhanced Thermal Conductivities From Lignin Nano-particles by Combining Hydrothermal Carbonization and Pyrolysis

Huiling Dong[1], Min Li[2], Yongcan Jin[2], Yan Wu[1], Caoxing Huang[2] and Jinlai Yang[3]**

[1] College of Furnishings and Industrial Design, Nanjing Forestry University, Nanjing, China, [2] Jiangsu Co-Innovation Center for Efficient Processing and Utilization of Forest Resources, Nanjing Forestry University, Nanjing, China, [3] Key Laboratory of High Efficient Processing of Bamboo of Zhejiang Province, China National Bamboo Research Center, Hangzhou, China

OPEN ACCESS

Edited by:
Li Shuai,
Fujian Agriculture and Forestry University, China

Reviewed by:
Chuan-Ling Si,
Tianjin University of Science and Technology, China
Rangana Jayawickramage,
Tomson Technologies LLC, United States

***Correspondence:**
Caoxing Huang
hcx@njfu.edu.cn
Jinlai Yang
5491936@163.com

Specialty section:
This article was submitted to Bioenergy and Biofuels, a section of the journal Frontiers in Energy Research

Received: *11 May 2020*
Accepted: *15 June 2020*
Published: *02 September 2020*

Citation:
Dong H, Li M, Jin Y, Wu Y, Huang C and Yang J (2020) Preparation of Graphene-Like Porous Carbons With Enhanced Thermal Conductivities From Lignin Nano-particles by Combining Hydrothermal Carbonization and Pyrolysis. Front. Energy Res. 8:148. doi: 10.3389/fenrg.2020.00148

Lignin nano-particles (LNPs) exhibit properties that distinguish them from the production of other lignin-based materials. However, little research has been performed to investigate whether porous carbons produced from LNPs exhibit a performance superior to those derived from untreated lignin. In this study, lignin was fabricated into LNPs and used to prepare high-performance porous carbons with enhanced thermal conductivities compared to that of carbons from neat lignin. Two different preparation protocols were employed: direct pyrolysis and hydrothermal carbonization followed by pyrolysis. Carbons obtained from 100 to 300 nm LNPs possessed more graphene-like structures than carbons from unaltered lignin. In addition, carbons prepared using a combination of hydrothermal carbonization and pyrolysis exhibited higher specific surface areas (108.81–220.75 m^2/g) and total pore volumes (0.098–0.166 cm^3/g) than those prepared via direct pyrolysis. In addition, LNP-derived carbons exhibited superior thermal conductivities (0.45 W/mK) and thermal conductivity rates (0.51°C/s). This work provides the useful finding that superior graphene-like porous carbons can be produced by transforming lignin into LNP and then hydrothermally carbonizing the resulting material prior to pyrolysis.

Keywords: lignin nano-particles, porous carbon, thermal conductivity, hydrothermal carbonization, graphene

INTRODUCTION

Graphene is a type of two-dimensional material composed of sp^2-structured monolayer carbon. Graphene continues to garner significant attention and utilization due to its extraordinary properties, such as its high theoretical surface area, exceptional thermal conductivity, and elevated Young's modulus (Lee et al., 2008; Yu et al., 2011). Based on these remarkable properties, graphene has been used to prepare materials including solar cells, high-performance supercapacitors, sensors and biosensors, polymer composite reinforcement fillers, and hydrogen storage materials (Hou et al., 2011; Huang et al., 2011; Sun et al., 2019). Various methods can be used to prepare graphene,

including the redox of graphene oxide, chemical vapor deposition, and surface separation of graphite (Xu et al., 2011; Liu et al., 2017). Although high-quality graphene can be obtained via the aforementioned methods, urgent technical and biological issues remain. These issues include a lack of mass production capacity, as well as environmental and human health concerns due to a reliance on toxic or hazardous reagents (Vlassiouk et al., 2013). To avoid these issues while maintaining the desired graphene properties, researchers have developed several graphene-like materials such as carbon nitride sheets, activated porous carbon (Ojha et al., 2017), carbon nanotubes (Araujo et al., 2012), and MoS_2 nanoplates (Hwang et al., 2011). These materials offer performances that are comparable to that of graphene for various applications.

Activated or porous carbons stand out among the previously mentioned graphene-like materials. This promising carbon material has tunable porosity, a large surface area, and intriguing electrical conductivity properties (Vinu, 2008). Depending on the preparation conditions and catalysts used, a variety of carbons can be fabricated to exhibit high specific surface areas and porosities that make them applicable as either high-performance supercapacitors or photocatalytic additives (Lv et al., 2015; Zhu et al., 2017; Foong et al., 2020). These carbons are generally produced from fossil sources such as coal and petroleum, or biomass sources such as rice husks, corn stalks, and bamboo residues (Abioye and Ani, 2015; Chen et al., 2018, 2019; Han et al., 2020). The material is generated from a feedstock via carbonization or pyrolysis, which are considered to have high techno-economic feasibilities due to their relatively low costs and good environmental compatibilities.

Of the various precursors used to prepare porous carbons, lignin is attractive because of its high carbon content (∼55–65%) and abundant supply from the pulp and paper industries. Lignin is a byproduct of wood pulp delignification (Pang et al., 2020b; Yoo et al., 2020). Dissolved lignin (typically in a solution called black liquor) is commonly burned to recover pulping chemicals and provide steam for power production (Shuai et al., 2016; Pang et al., 2020a). However, some manufacturers have begun to develop lignin products of lignosulphonate, adhesive, and foam as additional revenue streams for pulp and paper mills (Li and Ragauskas, 2012; Pang et al., 2020b; Pei et al., 2020). Lignin is also chemically well-suited to transformation into graphene-like porous carbons, particularly because they contain functional groups and have an abundance of benzene rings (Liu et al., 2017; Dong et al., 2020; Wang et al., 2020). In addition, the plentiful aromatic carbon atoms in the guaiacyl and syringyl groups in lignin are sp^2 hybridized, which is the basic unit of graphene (Liu et al., 2017). Hence, lignin is speculated to have great potential as a feedstock for activated carbon production. However, investigation of this topic has been limited.

Several methods have been investigated as a means of producing porous carbons with high specific surface areas and pore volumes from various biomass sources. In general, methods include physical activation (steam, CO_2, and air), chemical activation (H_3PO_4, $ZnCl_2$, and KOH), and combined physicochemical methods (Kılıç et al., 2015; Salehin et al., 2015; Demiral et al., 2016). The chemicals used in these processes inevitably cause environmental pollution and equipment corrosion. Hence, physical treatments are the preferred facile, green approaches to producing porous carbon. High pressure homogeneous (HPH) technology is a conventional approach that offers high efficiency, reproducibility, and ease of industrial scale-up (Donsi et al., 2010). It has been reported that HPH technology can be regarded as nanotechnology because of its ability to prepare nano-scale products (e.g., nano-crystalline cellulose and nano-lignin particles) from biomass resources (Li et al., 2012). All of these nano-scale products exhibit interesting properties, such as high mechanical strengths, large specific surface areas, and low thermal properties. We hypothesize that the use of nano-lignin particles as a feedstock may generate porous carbons with better performance than those derived from untreated lignin. Importantly, no work has been done to investigate such materials as precursors for porous carbon preparation.

The high thermal conductivity of graphene suggests that it can be applied to microelectronics and thermal management. Since Balandin (2011) discovered that graphene exhibited remarkably better thermal conductivity than conventional carbon nanotubes, graphene has been applied to heat management of high-power electronics, including thermal dissipation systems for chips and batteries in smartphones, tablets, smart VR systems, and wearable devices (Wu et al., 2019; Zheng et al., 2019; Yang et al., 2020). Many studies have shown that polymer composite thermal conduction capabilities can be improved significantly via the blending or grafting of graphene (Yu et al., 2007; Ji et al., 2014). Hence, if graphene-like carbon prepared from lignin exhibits better thermal conductivity than lignin, it may be valuable as a thermally conductive filler for polymer composites.

In this study, porous carbons were produced from both kraft lignin and lignin nano-particles (LNPs) in an effort to investigate whether the differences between these raw materials could positively affect the properties of the resulting materials. Porous carbons were pyrolyzed via two protocols: one-step direct pyrolysis and a two-step procedure in which hydrothermal carbonization was performed prior to pyrolysis. The resulting carbon samples were characterized using various instruments. The thermal conductivities of the prepared carbons were analyzed using an infrared thermal imager. This work investigates processing variables that can be applied to lignin carbonization in order promote the valorization of lignin.

MATERIALS AND METHODS

Materials

The kraft lignin used in this study was obtained from bamboo black liquor via acid precipitation according to the method in our previous work (Huang et al., 2019a,b; Lin et al., 2020). The obtained lignin was purified by diethyl ether. After purification, a lignin suspension was prepared by adding the lignin powder to distilled water at a solids content of 0.5% (w/w). The suspension was then homogenized using a laboratory high-pressure homogenizer at 30°C and 500 bar to obtain LNP.

All chemicals were purchased from their manufacturers and were used without further purification.

Fabrication of Carbon From Lignin

Two protocols were used to fabricate porous carbon from LNP and precipitated lignin. The first procedure (protocol 1) was a one-step method in which powdered materials were placed in a ceramic ark. This ark was then loaded into a tube furnace and subjected to pyrolysis under nitrogen. The heating procedure was as follows: (1) heating from 30 to 180°C at 2°C/min, followed by 1 h at the final temperature; (2) heating from 180 to 450°C at 2°C/min, followed by 1 h at the final temperature; and (3) heating from 450 to 1100°C at 2°C/min, with the final temperature maintained for 3 h. The carbons produced from untreated lignin and LNP were termed GN-1-LIN and GN-1-LNP, respectively.

The second procedure (protocol 2) involved two steps. First, a lignin solution (20 g in 100 g of water) was hydrothermally carbonized at 250°C and 150 MPa for 3 h. The resulting hydrothermally carbonized solids were then subjected to pyrolysis using the same tube furnace and heating procedure as protocol 1. The pyrolyzed carbons produced from untreated lignin and LNP were termed GN-2-LIN and GN-2-LNP, respectively.

Characterization

Lignin and prepared carbon morphologies were characterized using scanning (SEM, S4800, Hitachi, Japan) and transmission electron microscopy (TEM, JEM 2100, JEOL Ltd., Japan) at accelerating voltages of 200 and 15 kV, respectively. Fourier transform infrared (FTIR) analysis was performed using a Nicolet 6700 spectrometer (Nicolet Instrument Company, United States). Signals were recorded over a scanning range of 4000–400 cm^{-1}. X-ray diffraction (XRD) patterns were obtained using a diffractometer (Rigaku Ultima IV, Japan) and Cu Ka radiation. The operating parameters were a 40 kV voltage, 40 mA of current, a 5°/min scan speed, and a 2 theta range of 5°–80°. Raman spectra were obtained using a confocal Raman microscope (T64000, Horiba Scientific, France) with an excitation wavelength of 532 nm, power of 22 mW, integration time of 30 s, and three accumulations. X-ray photoelectron spectroscopy (XPS) was carried out by a Thermo Escalab spectrometer with an Al-K*a* ($h\nu$ = 1486.6 eV). Nitrogen adsorption and desorption were performed and the Brunauer–Emmett–Teller (BET) method was used to analyze the specific surface area using a Micromeritics ASAP 2020 instrument. Pore size distributions were evaluated via the Barrett–Joyner–Halenda method.

Thermal Conductivity Analysis

Thermal conductivity analysis was performed using a hot disk thermal constant analyzer (TPS 2500, Hot Disk AB Company, Sweden) via the transient plane heat source method. Temperature distribution images were captured using an infrared thermal imager during heating.

RESULTS AND DISCUSSION

Morphologies of Lignin and Graphene-Like Porous Carbons

Industrial kraft lignin is typically a powder with a microscopic three-dimensional structure (Dallmeyer et al., 2014). Fabrication of LNPs has been reported as an attractive avenue for generating new, valuable applications for lignin (Ma et al., 2019). In this study, a solvent-free, high-pressure homogeneous technology was used to fabricate LNP from kraft lignin. The purpose of this effort was to explore whether LNP could be pyrolyzed into graphene-like porous carbons with better properties than those made from untreated lignin. Lignin and LNP morphologies were observed via SEM and TEM and are shown in **Figures 1a,b**, **2a,b**, respectively.

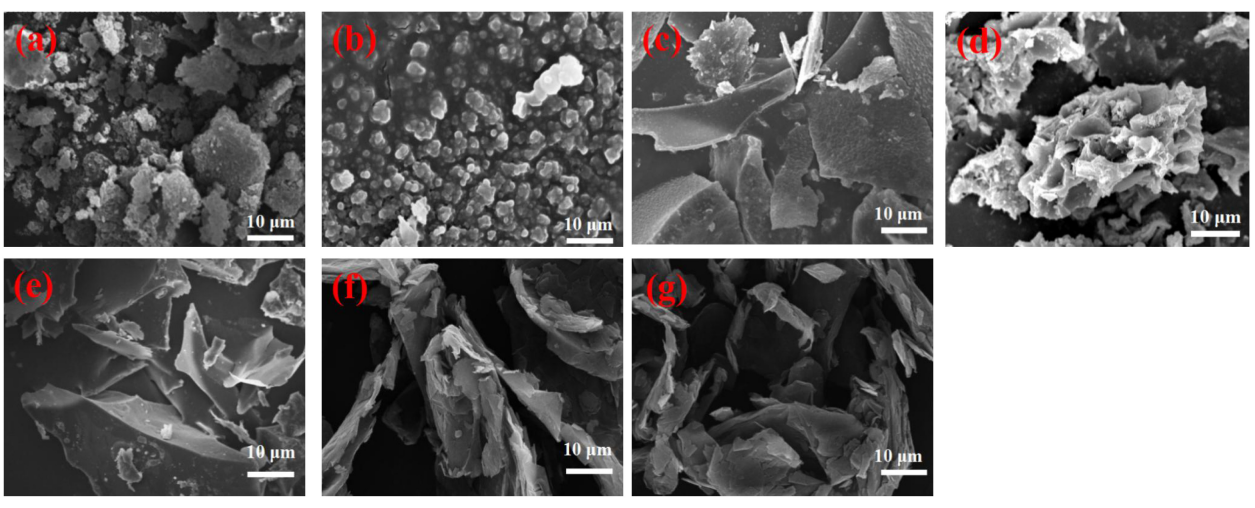

FIGURE 1 | SEM images of kraft lignin **(a)**, LNP **(b)**, and prepared carbons GN-1-LIN **(c)**, GN-2-LIN **(d)**, GN-1-LNP **(e)**, GN-2-LNP **(f)**, and commercial graphene **(g)**.

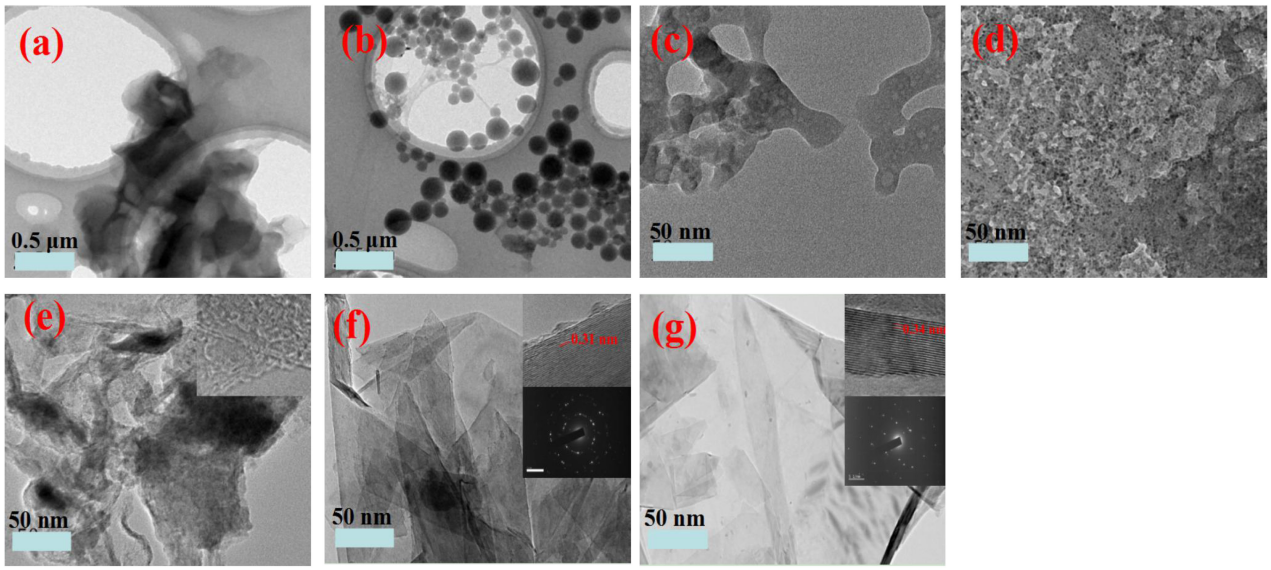

FIGURE 2 | TEM images of kraft lignin **(a)**, LNP **(b)**, and prepared carbons GN-1-LIN **(c)**, GN-2-LIN **(d)**, GN-1-LNP **(e)**, GN-2-LNP **(f)**, and commercial graphene **(g)**.

Figure 1a shows that neat lignin has a disordered micro-structure comprised of various shapes. **Figure 1b** shows that the LNPs produced are spherical particles with mostly uniform morphologies. Similar results are seen via TEM (**Figure 2b**). Nano-particle sizes are in the 100–300 nm range. Interestingly, this is similar to the sizes of LNPs derived from commercial lignin using solvent (tetrahydrofuran and dimethylsulfoxide) exchange and sonication (Ma et al., 2019; Sipponen et al., 2019).

Both lignin and LNP were used as precursors for preparation of four different activated carbons via two different production protocols. The morphologies of the prepared carbons were observed via SEM and TEM and are shown in **Figures 1c–f**, **2c–f**, respectively. In **Figures 1c,d**, agglomerated architectures of thick flakes and particles are observed from GN-1-LIN (first protocol) and GN-2-LIN (second protocol) carbons made from untreated lignin. This observation is in agreement with the work of Foong et al. (2020). It can also be seen that the formation of sheet-like surfaces is generally favored among LNP-derived carbons. Specifically, carbons made from LNPs via protocol 1 (GN-1-LNP) and protocol 2 (GN-2-LNP) exhibit prominent wrinkled surface textures with curling and sharp edges (**Figures 1e,f**). These properties are intrinsic graphene features of graphene, which can be more clearly observed in commercial graphene (**Figure 1g**). It is well known that corrugation and scrolling of the lamellae and edges are intrinsic graphene properties, which can clearly be observed in the TEM image of commercial graphene (**Figure 2g**; Barone et al., 2006; Tang et al., 2013). These properties were absent in the TEM images of carbons made from lignin (**Figures 2c,d**). **Figure 2e** showed that GN-1-LNP possessed some lamellae and edges similar to graphene, which can more clearly observed in the TEM image of GN-2-LNP (**Figure 2f**). The GN-2-LNP shows the in-plane lattice spacing of 0.31 nm corresponding to the (0 0 2) and (0 0 2) planes, and the spacing is closer to the 0.34 nm of graphene. Meanwhile, the GN-2-LNP shows a more similar diffraction pattern to the graphene, indicating the GN-2-LNP has a more similar polycrystalline structure with the graphene. According to the aforementioned results, it can be seen that the LNP-based carbons produced via protocol 2 contain more desirable features, such as smooth surfaces with creases and multi-layers with thin lamels (**Figure 2f**), than those produced via protocol 1. These results indicate that the combination of hydrothermal carbonization and pyrolysis generates porous carbons with greater morphological similarity to graphene-like structures than pyrolysis alone.

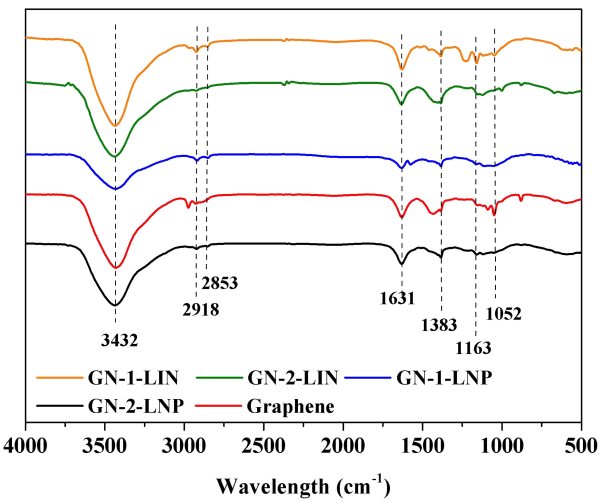

FIGURE 3 | FTIR spectra of the prepared carbons and commercial graphene.

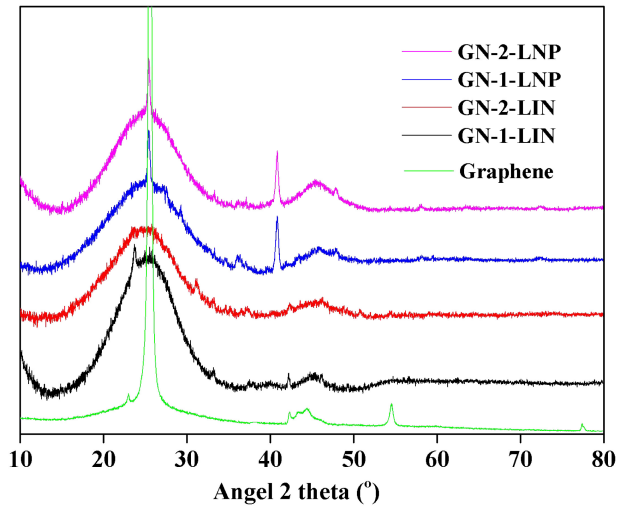

FIGURE 4 | XRD patterns of the prepared carbons and commercial graphene.

FTIR Spectra of Prepared Graphene-Like Porous Carbons

Fourier transform infrared was used to investigate the differences between the chemical structures of the porous carbons that we prepared and commercial graphene. The FTIR spectra are shown in **Figure 3**. The obvious peak at 1631 cm^{-1} is attributed to the graphene sheet C=C skeletal vibration (Song et al., 2012). The broad intense bands around 3432 and 1163 cm^{-1} correspond to the stretching vibrations of O–H and C–O functional groups, respectively, at the edges of graphene (Fernandes et al., 2018). The vibration peaks at 2918 and 2853 cm^{-1} correspond to the symmetric and antisymmetric stretching vibrations of CH_2 groups in graphene (Spitalsky et al., 2011). Importantly, the main graphene peaks are also visible without shifts in the FTIR spectra of our porous carbons. This indicates that graphene-like structures may be formed in lignin-based carbons manufactured using our protocols.

XRD Patterns of Prepared Graphene-Like Porous Carbons

X-ray diffraction patterns are an effective way to study the crystalline structures and layers comprising graphene (Morgan and Gilman, 2003; Vinodhkumar et al., 2018). The XRD spectra of the prepared carbons were obtained and compared to that of commercial graphene (**Figure 4**). It is well known that the (0 0 2) plane of graphene can exhibit a sharp reflection at $2\theta = 25.5°$ (Vinodhkumar et al., 2018). In **Figure 4**, both peaks at 25.6° are found in the patterns of commercial graphene, GN-1-LNP, and GN-2-LNP samples. This indicates that these carbons contain stacked graphene layers. However, GN-1-LIN and GN-2-LIN exhibit broad (0 0 2) graphitic plane diffraction peaks that are slightly shifted to a lower angle of 24.5°. In addition, GN-1-LNP and GN-2-LNP exhibit sharper (0 0 2) plane intensities than GN-1-LIN and GN-2-LIN. The work of Yan et al. (2018) also found that the degree of lignin graphitization can be improved via application of a treatment that forms nanoparticles. However, it should be pointed out that the XRD spectra of lignin derived

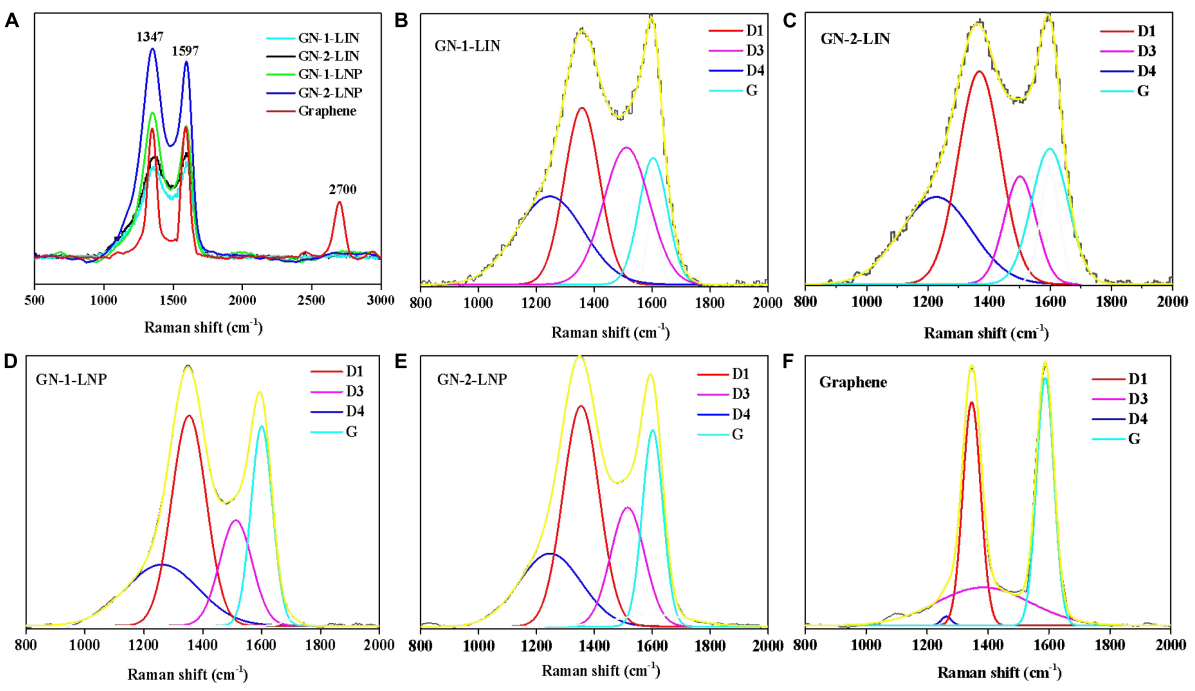

FIGURE 5 | Raman spectra of the prepared carbons and commercial graphene **(A)**, deconvoluted Raman spectra of GN-1-LIN **(B)**, GN-2-LIN **(C)**, GN-1-LNP **(D)**, GN-2-LNP **(E)**, and commercial graphene **(F)**.

carbons shows broader peaks than that of commercial graphene at around 25°. This can be explained as the lignin-derived carbons show small sheets and relatively low crystal structure, which are the inherent characteristics of biomass-based carbon materials that can show the broader (0 0 2) peaks around 25° (Han et al., 2017; Liu et al., 2017). Overall, from the aforementioned results, it can be seen that LNP appears to be the ideal starting material for the preparation of porous carbon based on the similarity of the resulting graphene-like structures to those in commercial graphene.

Raman Spectroscopy of Graphene-Like Porous Carbons

The aforementioned FTIR and XRD analyses reveal that the prepared carbons possess graphene-like structures. However, these results do not help one to understand specific differences between carbons that correlate with performance. Hence, Raman spectroscopy, a technology used to investigate edge strain and defects in graphene and graphitic materials (Vinu, 2008), was used to analyze the prepared porous carbons and commercial graphene.

Figure 5A shows that graphene exhibits two strong peaks at 1347 and 1597 cm^{-1}, which are attributed to the characteristic graphene D- and G-bands, respectively (Vinodhkumar et al., 2018; Sun et al., 2019). The G band is typically an in-plane stretching vibration of sp^2 hybrid carbon atoms in graphene. The D band is derived from disorder or defect vibration peaks in graphene (Dresselhaus et al., 2010; Sun et al., 2019). It can also represent a ring adjacent to a graphene edge or defect. **Figure 5** shows that the prepared carbons also exhibit G- and D-band vibrations. These edge strain and defect commonalties indicate that the prepared carbons exhibit structural properties analogous to those of graphene.

TABLE 1 | The I_D/I_G ratios, pore structures, and thermal conductivities of lignin, LNP, and the prepared carbons.

	I_{D1}/I_G	Specific surface area (m^2/g)	Total pore volume (cm^3/g)	Thermal conductivity (W/mK)	Amount of C–C in the C 1s (%)
GN-1-LIN	1.62	62.26	0.061	0.21	31.8
GN-2-LIN	1.77	108.81	0.098	0.22	31.8
GN-1-LNP	1.66	67.95	0.063	0.25	41.9
GN-2-LNP	1.36	220.75	0.166	0.45	49.5
graphene	0.93	/	/	/	49.6
lignin	/	18.78	0.027	0.11	/
LNP	/	30.35	0.045	0.18	/

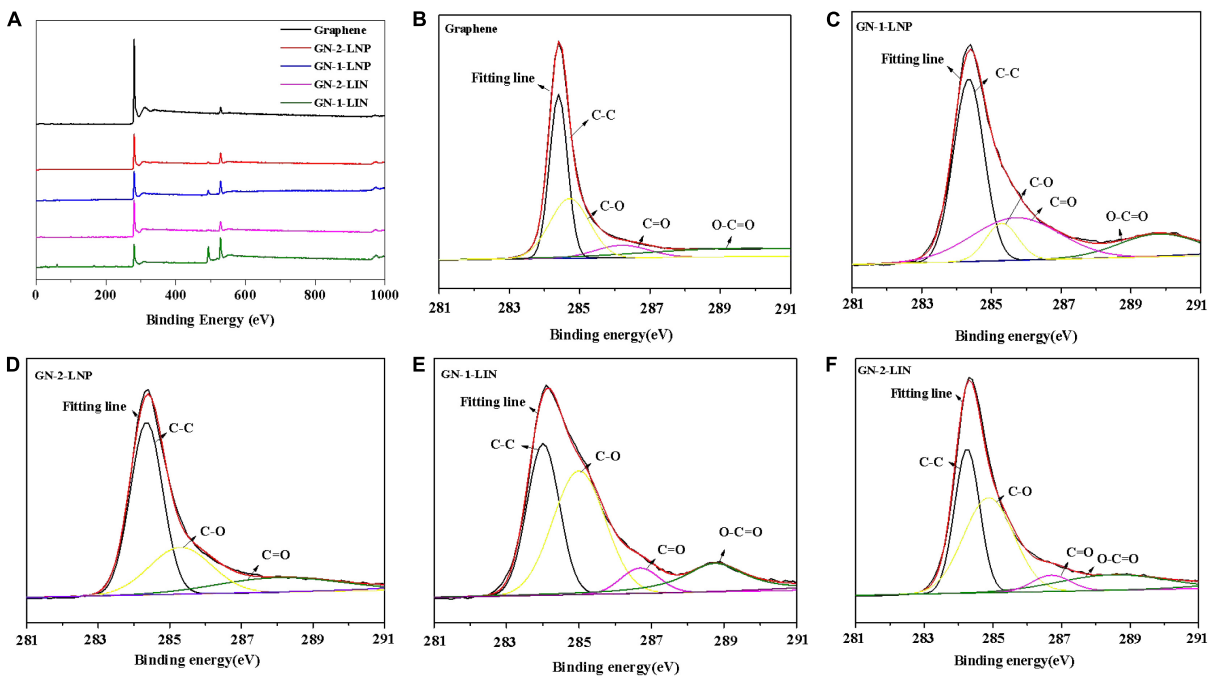

FIGURE 6 | XPS spectra of the prepared carbons and commercial graphene **(A)**, deconvoluted C 1s spectra of commercial graphene **(B)**, GN-1-LNP **(C)**, GN-2-LNP **(D)**, GN-1-LIN **(E)**, and GN-2-LIN **(F)**.

In Raman spectroscopy, the intensity of the G band can be used to determine the graphene thickness (Foong et al., 2020). **Figure 5A** shows that GN-1-LNP exhibits the same intensity as commercial graphene, which is lower than that of GN-2-LNP. These intensities indicate that the carbon derived from LNP via a combination of hydrothermal carbonization and pyrolysis possesses more graphene layers. The deconvolutions of Raman spectra are applied for all samples, and four Lorentzian functions are used to fit the D1, G, D3, and D4 bands (Lu et al., 2020), as shown in **Figures 5B–F**. In the fitted curves, D1-band and G-band are representative of the sp^2 hybridized carbon with structural defects or at plane edges and sp^2 hybridized carbon bond stretching in an ideal graphitic lattice (Hoekstra et al., 2016). Hence, the intensities ratio between the D1-band and G-band (I_{D1}/I_G) is indicative of the degree of graphitization (Dresselhaus et al., 2010; Liu et al., 2017; Lu et al., 2020). As shown in **Table 1**, the I_{D1}/I_G ratio of graphene is 0.93, which is lower than those of GN-1-LIN (1.62), GN-2-LIN (1.77), GN-1-LNP (1.66), and GN-2-LNP (1.36). These results indicate that using nano-particular lignin as a starting material can decrease the extent of disorder and defects in the prepared carbons, compared to that from the untreated lignin. Hence, it is hypothesized that the nano-lignin subjected to a combination of hydrothermal carbonization and pyrolysis possesses showed the potential ability to prepare the carbons with an enhanced degree of graphitization.

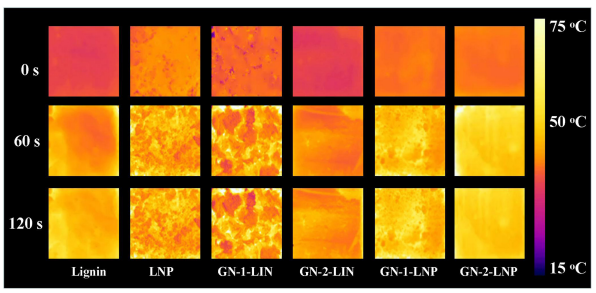

FIGURE 7 | Temperature distributions in the samples during heating.

XPS Spectroscopy of Graphene-Like Porous Carbons

To further understand the elemental composition of samples, the XPS spectra were obtained and shown in **Figure 6**. The survey XPS spectrum of the prepared porous carbons and commercial graphene (**Figure 6A**) shows strong peaks of C 1s at 284.4 eV and O 1s at 530.1 eV. The high resolution C 1s spectra (**Figures 6C–F**) showed the prepared carbons have two types of carbon, graphitic carbon (C–C) and oxygenated carbon (C–O, C=O, and O–C=O), which are also found in the C 1s curves of commercial graphene at the same binding energy (**Figure 6B**). The deconvolution of the C 1s can provide the relative amount of C–C (sp^2) in the sample (Kang et al., 2017). As shown in **Table 1**, the amount of C–C in commercial graphene was 49.6%, which was higher than those of GN-1-LIN (31.8%), GN-2-LIN (31.8%), GN-1-LNP (41.9%), and GN-2-LNP (49.5%). Among the prepared carbons, GN-2-LNP possessed the highest value of the relative amount of C–C, indicating it had the better graphitization (Mendes et al., 2020). These results are in accordance with the results from Raman analysis, which again indicate that using the combination of hydrothermal carbonization and pyrolysis show more potential to prepare the carbon with an enhanced degree of graphitization from nano-lignin than that from untreated lignin.

Pore Structure Analysis of Prepared Graphene-Like Porous Carbons

In this study, we sought to prepare porous carbons from LNP that are more similar to graphene than those prepared from untreated lignin. To further investigate the pore structures of the prepared carbons, N_2 sorption and desorption isotherms were measured. The BET model is used to calculate the specific surface areas shown in **Table 1**.

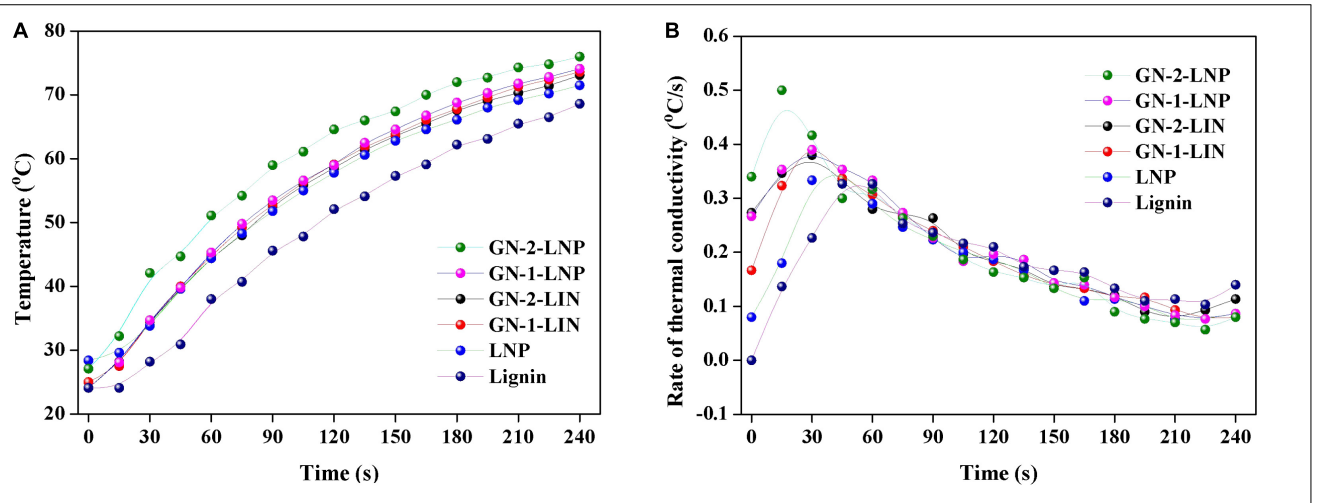

FIGURE 8 | (A) Real-time temperature and **(B)** rate of thermal conductivity curves.

Table 1 shows that the BET specific surface area and pore volume of lignin are 18.75 and 0.027 cm^3/g, respectively. These values increase to 30.35 and 0.045 cm^3/g once a sample is homogenized to form LNP. The carbons obtained via protocol 1, GN-1-LIN and GN-1-LNP, both exhibit similar BET specific surface areas (62.26 and 67.95 m^2/g, respectively) and pore volumes (0.061 and 0.063 cm^3/g, respectively). In contrast, protocol 2 (hydrothermal carbonization followed by pyrolysis) clearly produces porous carbons with larger surface areas and pore volumes. The BET specific surface area and pore volume of GN-2-LIN are 108.81 and 0.098 cm^3/g, respectively. Those of GN-2-LNP are 220.75 and 0.166 cm^3/g, respectively. These results indicate that the application of hydrothermal carbonization prior to pyrolysis produces better pore structures than pyrolysis alone. In addition, GN-2-LNP exhibits better pore structure properties than GN-2-LIN, which indicates that LNP has more potential than lignin for porous carbon production. This phenomenon may be explained by pore structure enlargement by flake- and sheet-like structures in GN-2-LNP. A similar finding was reported by Ojha et al. (2017). Although the BET specific surface area of GN-2-LNP are lower than those reported for carbons (1100 and 3775 m^2/g) in the aforementioned work (Zhang et al., 2015; Hu and Hsieh, 2017), our results are valuable because they reveal that nano-scale lignin and the combination of hydrothermal carbonization and pyrolysis show more potential for porous carbon preparation.

Analysis of the Thermal Conduction Capabilities of Prepared Graphene-Like Porous Carbons

It is well known that graphene exhibits better thermal conductivity than other thermally conductive materials (Yu et al., 2011). This has supported its use in modern electronics and other daily necessities. As the prepared carbons derived from the nano-lignin possessed the graphene like structures, it is important to also evaluate the thermal conductivity of lignin-derived carbons if they are intended to prepare the conductivity-based materials. The thermal conductivities of all samples are shown in **Table 1**. In addition, thermal images of samples taken during heating are shown in **Figure 7**. Finally, real-time temperature curves and thermal conductivity rate curves derived during heating are shown in **Figures 8A,B**, respectively.

Table 1 shows that GN-1-LIN and GN-2-LIN exhibit similar thermal conductivities (0.21 W/mK). This value is slightly improved to 0.28 W/mK in a carbon prepared from LNP using protocol 1. However, the thermal conductivity increases significantly from 0.22 W/mK to 0.45 W/mK when the carbon is prepared from LNP using protocol 2. This increase is also observed via the infrared thermal images in **Figure 7**, which show the temperature responses that occur during heating of GN-2-LIN and GN-2-LNP. The temperature of GN-2-LNP increases much more rapidly than that of GN-2-LIN, which indicates that the former material has a higher thermal conductivity. Overall, it can be concluded that the LNP treated by protocol 2 showed a higher ability to prepare the carbons with enhanced thermal conductivity.

Thermal conductivity rate curves, which are derived from the real-time temperature curves in **Figure 8A**, are shown in **Figure 8B**. GN-2-LNP exhibits the highest rate of thermal conductivity (0.51°C/s at 15 s). This is higher than those of the other three samples at double the time (0.38°C/s at 30 s). This means that GN-2-LNP has the best thermal diffusion capabilities of the prepared carbons. This superior performance might be due to its higher proportion of graphene-like structures (Yu et al., 2011). Overall, the thermal conduction ability analysis reveals that the graphene-like carbon made from nano-scale lignin has better thermal conduction capabilities than the carbon made from un-treated lignin. This is in line with our initial expectations. The higher thermal conduction rate of GN-2-LNP indicates that it has potential thermal management applications.

CONCLUSION

Lignin nano-particles with a size range of 100–300 nm were prepared from lignin using a high-pressure homogenizer with the intention of fabricating them into graphene-like carbon. LNP treated by a combination of hydrothermal carbonization and pyrolysis showed more potential for porous carbon based on its high proportion of graphene-like structures and degree of graphitization. Application of hydrothermal carbonization prior to pyrolysis made a strong contribution to the resultant carbon's higher specific surface areas and total pore volume. In addition, the LNP showed a better capacity to prepare the carbon with higher thermal conductivity (0.45 W/mK) and rate of thermal conductivity (0.51°C/s) compared to un-treated lignin.

DATA AVAILABILITY STATEMENT

The raw data supporting the conclusions of this article will be made available by the authors, without undue reservation.

AUTHOR CONTRIBUTIONS

HD carried out all the experiments and wrote the manuscript. ML and YW performed the data analysis. YJ, CH, and JY designed the work and revised the manuscript. All authors discussed the results.

FUNDING

This work was supported by the National Natural Science Foundation of China (31730106) and Natural Science Foundation of Jiangsu Province (BK20180772).

REFERENCES

Abioye, A. M., and Ani, F. N. (2015). Recent development in the production of activated carbon electrodes from agricultural waste biomass for supercapacitors: a review. *Renew. Sust. Energ. Rev.* 52, 1282–1293. doi: 10.1016/j.rser.2015.07.129

Araujo, P. T., Terrones, M., and Dresselhaus, M. S. (2012). Defects and impurities in graphene-like materials. *Mater. Today* 15, 98–109. doi: 10.1016/S1369-7021(12)70045-7

Balandin, A. A. (2011). Thermal properties of graphene and nanostructured carbon materials. *Nat. Mater.* 10, 569–581. doi: 10.1038/nmat3064

Barone, V., Hod, O., and Scuseria, G. E. (2006). Electronic structure and stability of semiconducting graphene nanoribbons. *Nano Lett.* 6, 2748–2754. doi: 10.1021/nl0617033

Chen, D., Gao, A., Ma, Z., Fei, D., Chang, Y., and Shen, C. (2018). In-depth study of rice husk torrefaction: characterization of solid liquid and gaseous products oxygen migration and energy yield. *Bioresource Technol.* 253, 148–153. doi: 10.1016/j.biortech.2018.01.009

Chen, D., Wang, Y., Liu, Y., Cen, K., Cao, X., Ma, Z., et al. (2019). Comparative study on the pyrolysis behaviors of rice straw under different washing pretreatments of water acid solution and aqueous phase bio-oil by using TG-FTIR and Py-GC/MS. *Fuel* 252, 1–9. doi: 10.1016/j.fuel.2019.04.086

Dallmeyer, I., Lin, L. T., Li, Y., Ko, F., and Kadla, J. F. (2014). Preparation and characterization of interconnected kraft lignin-based carbon fibrous materials by electrospinning. *Macromol. Mater. Eng.* 299, 540–551. doi: 10.1002/mame.201300148

Demiral, I., Aydın Şamdan, C., and Demiral, H. (2016). Production and characterization of activated carbons from pumpkin seed shell by chemical activation with ZnCl2. *Water Treat.* 57, 2446–2454. doi: 10.1080/19443994.2015.1027276

Dong, H., Zheng, L., Yu, P., Jiang, Q., Wu, Y., Huang, C., et al. (2020). Characterization and application of lignin-carbohydrate complexes from lignocellulosic materials as antioxidants for scavenging in vitro and in vivo reactive oxygen species. *ACS Sustain. Chem. Eng.* 8, 256–266. doi: 10.1021/acssuschemeng.9b05290

Donsi, F., Wang, Y., Li, J. I, and Huang, Q. (2010). Preparation of curcumin submicrometer dispersions by high-pressure homogenization. *J. Agr. Food Chem.* 58, 2848–2853. doi: 10.1021/jf903968x

Dresselhaus, M. S., Jorio, A., Hofmann, M., Dresselhaus, G., and Saito, R. (2010). Perspectives on carbon nanotubes and graphene Raman spectroscopy. *Nano Lett.* 10, 751–758. doi: 10.1021/nl904286r

Fernandes, D. M., Araújo, M. P., Haider, A., Mougharbel, A. S., Fernandes, A. J., Kortz, U., et al. (2018). Polyoxometalate-graphene electrocatalysts for the hydrogen evolution reaction. *ChemElectroChem* 5, 273–283. doi: 10.1002/celc.201701210

Foong, L. K., Khojasteh, H., Amiri, M., Heydaryan, K., Salavati-Niasari, M., Almasi-Kashi, M., et al. (2020). Environmental friendly approach for facile synthesis of graphene-like nanosheets for photocatalytic activity. *J. Alloy Compd.* 823:153696. doi: 10.1016/j.jallcom.2020.153696

Han, H., Chao, S., Yang, X., Wang, X., Wang, K., Bai, Z., et al. (2017). Ni nanoparticles embedded in N doped carbon nanotubes derived from a metal organic framework with improved performance for oxygen evolution reaction. *Int. J. Hydrogen Energ.* 42, 16149–16156. doi: 10.1016/j.ijhydene.2017.05.043

Han, H., Lou, Z., Wang, P., Wang, Q., Li, R., Zhang, Y., et al. (2020). Synthesis of Ultralight and Porous Magnetic g-C3N4/g-Carbon Foams with Excellent Electromagnetic Wave (EMW) Absorption Performance and Their Application as a Reinforcing Agent for 3D Printing EMW Absorbers. *Ind. Eng. Chem. Res.* 59, 7633–7645. doi: 10.1021/acs.iecr.0c00665

Hoekstra, J., Beale, A. M., Soulimani, F., Versluijs-Helder, M., Van De Kleut, D., Koelewijn, J. M., et al. (2016). The effect of iron catalyzed graphitization on the textural properties of carbonized cellulose: magnetically separable graphitic carbon bodies for catalysis and remediation. *Carbon* 107, 248–260. doi: 10.1016/j.carbon.2016.05.065

Hou, J., Shao, Y., Ellis, M. W., Moore, R. B., and Yi, B. (2011). Graphene-based electrochemical energy conversion and storage: fuel cells supercapacitors and lithium ion batteries. *Phys. Chem. Chem. Phys.* 13, 15384–15402. doi: 10.1039/C1CP21915D

Hu, S., and Hsieh, Y. L. (2017). Lignin derived activated carbon particulates as an electric supercapacitor: carbonization and activation on porous structures and microstructures. *RSC Adv.* 7, 30459–30468. doi: 10.1039/C7RA00103G

Huang, C., Lin, W., Lai, C., Li, X., Jin, Y., and Yong, Q. (2019a). Coupling the post-extraction process to remove residual lignin and alter the recalcitrant structures for improving the enzymatic digestibility of acid-pretreated bamboo residues. *Bioresource Technol.* 285:121355. doi: 10.1016/j.biortech.2019.121355

Huang, C., Wang, X., Liang, C., Jiang, X., Yang, G., Xu, J., et al. (2019b). A sustainable process for procuring biologically active fractions of high-purity xylooligosaccharides and water-soluble lignin from Moso bamboo prehydrolyzate. *Biotechnol. Biofuels* 12:189. doi: 10.1186/s13068-019-1527-3

Huang, X., Yin, Z., Wu, S., Qi, X., He, Q., Zhang, Q., et al. (2011). Graphene-based materials: synthesis characterization properties and applications. *Small* 7, 1876–1902. doi: 10.1002/smll.201002009

Hwang, H., Kim, H., and Cho, J. (2011). MoS2 nanoplates consisting of disordered graphene-like layers for high rate lithium battery anode materials. *Nano Lett.* 11, 4826–4830. doi: 10.1021/nl202675f

Ji, H., Sellan, D. P., Pettes, M. T., Kong, X., Ji, J., Shi, L., et al. (2014). Enhanced thermal conductivity of phase change materials with ultrathin-graphite foams for thermal energy storage. *Energ. Environ. Sci.* 7, 1185–1192. doi: 10.1039/C3EE42573H

Kang, M. H., Qiu, G., Chen, B., Jouvray, A., Teo, K. B., Cepek, C., et al. (2017). Transport in polymer-supported chemically-doped CVD graphene. *J. Mater. Chem. C* 5, 9886–9897. doi: 10.1039/C7TC02263H

Kılıç, M., Apaydın-Varol, E., and Pütün, A. E. (2015). Preparation and surface characterization of activated carbons from Euphorbia rigida by chemical activation with ZnCl2 K2CO3 NaOH and H3PO4. *Appl. Surf. Sci.* 261, 247–254. doi: 10.1016/j.apsusc.2012.07.155

Lee, C., Wei, X., Kysar, J. W., and Hone, J. (2008). Measurement of the elastic properties and intrinsic strength of monolayer graphene. *Science* 321, 385–388. doi: 10.1126/science.1157996

Li, J., Wei, X., Wang, Q., Chen, J., Chang, G., Kong, L., et al. (2012). Homogeneous isolation of nanocellulose from sugarcane bagasse by high pressure homogenization. *Carbohyd. Polym.* 90, 1609–1613. doi: 10.1016/j.carbpol.2012.07.038

Li, Y., and Ragauskas, A. J. (2012). Kraft lignin-based rigid polyurethane foam. *J. Wood Chem. Technol.* 32, 210–224. doi: 10.1080/02773813.2011.652795

Lin, W., Xing, S., Jin, Y., Lu, X., Huang, C., and Yong, Q. (2020). Insight into understanding the performance of deep eutectic solvent pretreatment on improving enzymatic digestibility of bamboo residues. *Bioresource Technol.* 306:123163. doi: 10.1016/j.biortech.2020.123163

Liu, F., Chen, Y., and Gao, J. (2017). Preparation and characterization of biobased graphene from Kraft lignin. *Bioresources* 12, 6545–6557.

Lu, Y., Liu, Z., You, S. W., McLoughlin, L., Bridgers, B., Hayes, S., et al. (2020). Electrospun carbon/iron nanofibers: the catalytic effects of iron and application in Cr (VI) removal. *Carbon* 166, 227–244. doi: 10.1016/j.carbon.2020.05.031

Lv, B., Zheng, C., Xu, L., Zhou, X., Cao, H., and Liu, Z. (2015). Porous graphene-like materials prepared from hollow carbonaceous microspheres for supercapacitors. *ChemNanoMat* 1, 422–429. doi: 10.1002/cnma.201500081

Ma, M., Dai, L., Si, C., Hui, L., Liu, Z., and Ni, Y. (2019). Facile preparation of super long-term stable lignin nanoparticles from black liquor. *ChemSusChem* 12, 5239–5245. doi: 10.1002/cssc.201902287

Mendes, L. F., de Siervo, A., de Araujo, W. R., and Paixão, T. R. L. C. (2020). Reagentless fabrication of a porous graphene-like electrochemical device from phenolic paper using laser-scribing. *Carbon* 159, 110–118. doi: 10.1016/j.carbon.2019.12.016

Morgan, A. B., and Gilman, J. W. (2003). Characterization of polymer-layered silicate (clay) nanocomposites by transmission electron microscopy and X-ray diffraction: a comparative study. *J. Appl. Polym. Sci.* 87, 1329–1338. doi: 10.1002/app.11884

Ojha, K., Kumar, B., and Ganguli, A. K. (2017). Biomass derived graphene-like activated and non-activated porous carbon for advanced supercapacitors. *J. Chem. Sci.* 129, 397–404. doi: 10.1007/s12039-017-1248-8

Pang, B., Cao, X. F., Sun, S. N., Wang, X. L., Wen, J. L., Lam, S. S., et al. (2020a). The direct transformation of bioethanol fermentation residues for production of high-quality resins. *Green Chem.* 22, 439–447. doi: 10.1002/cssc.202000299

Pang, B., Lam, S. S., Shen, X. J., Cao, X. F., Liu, S. J., Yuan, T. Q., et al. (2020b). Valorization of technical lignin for production of desirable resins with high substitution rate and controllable viscosity. *ChemSusChem* 13, 1–10.

Pei, W., Shang, W., Liang, C. Jiang, X, Huang, C., and Yong, Q. (2020). Using lignin as the precursor to synthesize Fe_3O_4@lignin composite for preparing electromagnetic wave absorbing lignin-phenol-formaldehyde adhesive. *Ind. Crop. Prod.* 154:112638. doi: 10.1016/j.indcrop.2020.112638

Salehin, S., Aburizaiza, A. S., and Barakat, M. A. (2015). Recycling of residual oil fly ash: synthesis and characterization of activated carbon by physical activation methods for heavy metals adsorption. *Int. J. Environ. Res.* 9, 1201–1210. doi: 10.22059/IJER.2015.1010

Shuai, L., Amiri, M. T., Questell-Santiago, Y. M., Héroguel, F., Li, Y., Kim, H., et al. (2016). Formaldehyde stabilization facilitates lignin monomer production during biomass depolymerization. *Science* 354, 329–333. doi: 10.1126/science.aaf7810

Sipponen, M. H., Lange, H., Crestini, C., Henn, A., and Österberg, M. (2019). Lignin for nano- and microscaled carrier systems: applications trends and challenges. *ChemSusChem* 12, 2039–2054. doi: 10.1002/cssc.201900480

Song, C., Wu, D., Zhang, F., Liu, P., Lu, Q., and Feng, X. (2012). Gemini surfactant assisted synthesis of two-dimensional metal nanoparticles/graphene composites. *Chem. Commun.* 48, 2119–2121. doi: 10.1039/C2CC16890A

Spitalsky, Z., Danko, M., and Mosnacek, J. (2011). Preparation of functionalized graphene sheets. *Curr. Org. Chem.* 15, 1133–1150. doi: 10.2174/138527211795202988

Sun, S., Zhang, M., Umemura, K., and Zhao, Z. (2019). Investigation and characterization of synthesis conditions on sucrose-ammonium dihydrogen phosphate (SADP) adhesive: bond performance and chemical transformation. *Materials* 12:4078. doi: 10.3390/ma12244078

Tang, L. C., Wan, Y. J., Yan, D., Pei, Y. B., Zhao, L., Li, Y. B., et al. (2013). The effect of graphene dispersion on the mechanical properties of graphene/epoxy composites. *Carbon* 60, 16–27. doi: 10.1016/j.carbon.2013.03.050

Vinodhkumar, G., Ramya, R., Vimalan, M., Potheher, I., and Cyrac Peter, A. (2018). Reduced graphene oxide based on simultaneous detection of neurotransmitters. *Prog. Chem. Biochem. Res.* 1, 40–49.

Vinu, A. (2008). Two-dimensional hexagonally-ordered mesoporous carbon nitrides with tunable pore diameter surface area and nitrogen content. *Adv. Funct. Mater.* 18, 816–827. doi: 10.1002/adfm.200700783

Vlassiouk, I., Fulvio, P., Meyer, H., Lavrik, N., Dai, S., Datskos, P., et al. (2013). Large scale atmospheric pressure chemical vapor deposition of graphene. *Carbon* 54, 58–67. doi: 10.1016/j.carbon.2012.11.003

Wang, S., Li, H., Xiao, L. P., and Song, G. (2020). Unraveling the structural transformation of wood lignin during deep eutectic solvent treatment. *Front. Energy Res.* 8:48. doi: 10.3389/fenrg.2020.00048

Wu, Y., Wu, X., Yang, F., Xu, L., and Sun, M. (2019). Study on the preparation and adsorption property of polyvinyl alcohol/cellulose nanocrystal/graphene composite aerogels (PCGAs). *J. Renew. Mater.* 7, 1181–1195. doi: 10.32604/jrm.2019.07493

Xu, M., Fujita, D., Sagisaka, K., Watanabe, E., and Hanagata, N. (2011). Production of extended single-layer graphene. *ACS Nano* 5, 1522–1528. doi: 10.1021/nn103428k

Yan, Q., Zhang, X., Li, J., Wang, C., Zhang, J., and Cai, Z. (2018). Catalytic conversion of Kraft lignin to bio-multilayer graphene materials under different atmospheres. *J. Mater. Sci.* 53, 8020–8029. doi: 10.1007/s10853-018-2172-0

Yang, J. W., Yu, Z. Y., Cheng, S. J., Chung, J. H., Liu, X., Wu, C. Y., et al. (2020). Graphene oxide-based nanomaterials: an insight into retinal prosthesis. *Int. J. Mol. Sci.* 21:2957. doi: 10.3390/ijms21082957

Yoo, C. G., Meng, X., Pu, Y., and Ragauskas, A. J. (2020). The critical role of lignin in lignocellulosic biomass conversion and recent pretreatment strategies: a comprehensive review. *Bioresource Technol.* 2020:122784. doi: 10.1016/j.biortech.2020.122784

Yu, A., Ramesh, P., Itkis, M. E., Bekyarova, E., and Haddon, R. C. (2007). Graphite nanoplatelet-epoxy composite thermal interface materials. *J. Phys. Chem. C* 111, 7565–7569. doi: 10.1021/jp071761s

Yu, W., Xie, H., Wang, X., and Wang, X. (2011). Significant thermal conductivity enhancement for nanofluids containing graphene nanosheets. *Phys. Lett. A* 375, 1323–1328. doi: 10.1016/j.physleta.2011.01.040

Zhang, W., Zhao, M., Liu, R., Wang, X., and Lin, H. (2015). Hierarchical porous carbon derived from lignin for high performance supercapacitor. *Colloid Surface A* 484, 518–527. doi: 10.1016/j.colsurfa.2015.08.030

Zheng, C., Yue, Y., Gan, L., Xu, X., Mei, C., and Han, J. (2019). Highly stretchable and self-healing strain sensors based on nanocellulose-supported graphene dispersed in electro-conductive hydrogels. *Nanomaterials* 9:937. doi: 10.3390/nano9070937

Zhu, L., Shen, F., Smith, R. L. Jr., Yan, L., Li, L., and Qi, X. (2017). Black liquor-derived porous carbons from rice straw for high-performance supercapacitors. *Chem. Eng. J.* 316, 770–777. doi: 10.1016/j.cej.2017.02.034

Conflict of Interest: The authors declare that the research was conducted in the absence of any commercial or financial relationships that could be construed as a potential conflict of interest.